Langmuir
Article
pubs.acs.org/Langmuir

Valency Dependence of Polymorphism and Polyamorphism in DNA-Functionalized Nanoparticles

Wei Dai,[†] Chia Wei Hsu,[†] Francesco Sciortino,[‡] and Francis W. Starr*[,†]

[†]*Department of Physics, Wesleyan University, Middletown, Connecticut 06459, and* [‡]*Dipartimento di Fisica and CNR-INFM-SOFT: Complex Dynamics in Structured Systems, Università di Roma La Sapienza, Piazzale Aldo Moro 2, I-00185 Roma, Italy*

Received August 14, 2009. Revised Manuscript Received September 27, 2009

Nanoparticles (NP) functionalized with single-stranded DNA (ssDNA) offer a route to custom-designed, self-assembled nanomaterials with potentially unusual properties. The bonding selectivity of DNA guarantees one-to-one binding to form double-stranded DNA (dsDNA), and an appropriate base sequence results in head-to-tail binding linking NP into networks. We explore the phase behavior and structure of a model for NP functionalized with between 3 and 6 short ssDNA through simulations of a coarse-grained molecular model, allowing us to examine both the role of the number of attached strands (valency) and their relative orientations. The NP assemble into networks where the number of NP links is controlled by the number of attached strands. The large length scale of the DNA links relative to the core NP size opens the possibility for the formation of interpenetrating networks that give rise to multiple thermodynamically distinct states. We find that the 3-functionalized NP have only a single phase transition between a dilute solution of NPs and an assembled network state. 4-Functionalized NP (with tetrahedral symmetry) exhibit four amorphous phases, or polyamorphism, each higher density phase consisting of an additional interpenetrating network. The two investigated geometries of 5-functionalized NP both exhibit two phase transitions and three amorphous phases. Like the 4-functionalized NP, the highest density phase consists of interpenetrating networks, demonstrating that regular symmetry is not a prerequisite for interpenetration to produce thermodynamically distinct phases. The width of the coexistence regions for all phase transitions increases with increasing functionality. Finally, for 6-functionalized NP with octahedral symmetry, the possibility of observing disordered phases with significantly bonded particles is preempted by the formation of ordered crystal phases. Interestingly, the extreme softness of the potential combined with the directional interaction allows for the formation of (at least) six distinct crystalline structures (i.e., polymorphism) consisting of up to six interpenetrating simple cubic lattices.

1. Introduction

The application of biological constructions to artificially devised complexes holds great promise for the development of self-assembled nanostructures and materials.[1−3] Among the many choices, DNA is particularly attractive, as the bonding specificity and "lock-and-key" interactions offer a route to design highly organized materials through a synthetic bottom-up approach.[4−6] Complex DNA-based networks require the linear single strands (ssDNA) or double stands (dsDNA) to be linked by junctions, formed either by a branched DNA structure[7−9] or by linking the DNA to a vertex unit.[10] By grafting multiple ssDNA to core nanoparticles (NP), and an intelligent choice for the base sequence, DNA-functionalized NP link via the formation of dsDNA, and the NP act as nodes of a complex network. Experimentally, most studies of DNA-functionalized particles have explored uniform coverage of micrometer size colloids[11−15] or nanoscale gold NP.[16] While there has been success making ordered crystal structures,[15,17−19] such uniform coating makes it difficult to control the organization of higher order structures. If one can make an appropriate choice of geometry of the ssDNA attached to a core NP, or alternatively control the geometry of preassembled DNA macromolecules (e.g., the Holliday junction or synthetic junctions[20,21]), it should be possible to control the symmetries of the resulting structures.[22] Such controlled attachment points to a core NP have been achieved experimentally,[23,24] but examination of bulk material properties has so far only been

*To whom correspondence should be addressed. E-mail: fstarr@wesleyan.edu.

(1) Whitesides, G. M.; Wong, A. P. *MRS Bull.* **2006**, *31*, 19–27.
(2) Chan, G.; Mooney, D. J. *Trends Biotechnol.* **2008**, *26*, 382.
(3) Berti, D. *Curr. Opin. Colloid Interface Sci.* **2006**, *11*, 74–78.
(4) Niemeyer, C. M. *Curr. Opin. Chem. Biol.* **2000**, *4*, 609–618.
(5) Seeman, N. C. *Nature* **2003**, *421*, 427–431.
(6) Condon, A. *Nat. Rev. Genet.* **2006**, *7*, 565–575.
(7) Winfree, E.; Liu, F. R.; Wenzler, L. A.; Seeman, N. C. *Nature* **1998**, *394*, 539–544.
(8) He, Y.; Ye, T.; Su, M.; Zhang, C.; Ribbe, A. E.; Jiang, W.; Mao, C. *Nature* **2008**, *452*, 198–201.
(9) Endo, M.; Majima, T. *Chem. Commun.* **2006**, *22*, 2329–2331.
(10) Mirkin, C. A.; Letsinger, R. L.; Mucic, R. C.; Storhoff, J. J. *Nature* **1996**, *382*, 607–609.
(11) Valignat, M. P.; Theodoly, O.; Croker, J. C.; Russel, W. B.; Chaikin, P. M. *Proc. Natl. Acad. Sci. U.S.A.* **2005**, *102*, 4225–4229.
(12) Biancaniello, P. L.; Kim, A. J.; Crocker, J. C. *Phys. Rev. Lett.* **2005**, *94*, 058302.
(13) Schmatko, T.; Bozorgui, B.; Geerts, N.; Frenkel, D.; Eiser, E.; Poon, W. C. K. *Soft Matter* **2007**, *3*, 703–706.
(14) Geerts, N.; Schmatko, T.; Eiser, E. *Langmuir* **2008**, *24*, 5118–5123.
(15) Kim, A. J.; Scarlett, R.; Biancaniello, P. L.; Sinno, T.; Crocker, J. C. *Nat. Mater.* **2009**, *8*, 52–55.
(16) Harris, N. C.; Kiang, C.-H. *Phys. Rev. Lett.* **2005**, *95*, 046101.
(17) Park, S. Y.; Lytton-Jean, A. K. R.; Lee, B.; Weigand, S.; Schatz, G. C.; Mirkin, C. A. *Nature* **2008**, *451*, 553–556.
(18) Nykypanchuk, D.; Maye, M. M.; van der Lelie, D.; Gang, O. *Nature* **2008**, *451*, 549–552.
(19) Xiong, H.; van der Lelie, D.; Gang, O. *Phys. Rev. Lett.* **2009**, *102*, 015504.
(20) Endo, M.; Seeman, N. C.; Majima, T. *Angew. Chem.* **2005**, *44*, 6074–6077.
(21) Endo, M.; Shiroyama, T.; Fujitsuka, M.; Majima, T. *J. Org. Chem.* **2005**, *70*, 7468–7472.
(22) Glotzer, S. C.; Solomon, M. C. *Nat. Mater.* **2007**, *6*, 557–562.
(23) Stewart, K. M.; McLaughlin, L. W. *J. Am. Chem. Soc.* **2004**, *126*, 2050–2057.
(24) Stewart, K. M.; Rojo, J.; McLaughlin, L. W. *Angew. Chem.* **2004**, *43*, 5808–5811.

realized through computer simulation.[25−27] Here, we take advantage of the control offered by simulations to address the role of the number of attached DNA strands on the macroscopic behavior via a coarse-grained molecular model.

Unlike uniformly functionalized NP, systems with a limited bonding coordination, or valency, readily form a homogeneous low-density state with significant empty space in the network.[28] NP with a specified number of attached ssDNA (i.e., valency) can have near vanishing densities, since the length scale of the DNA bonding "arms" can be large as compared with the core NP size, even when the length of the DNA sequence is below the dsDNA persistence length. For the case of tetrahedrally functionalized NP, the units can assemble into a large-scale amorphous network with locally tetrahedral order.[25−27] Moreover, since vast empty spaces exist and are locally tetrahedral, it is possible to repeat the motif with a second locally tetrahedral network occupying the unoccupied space of the first network. Within the investigated length of the DNA sequences (less than 16 base pairs), this process can be repeated a third time, and at low temperature, these networked states become thermodynamically distinct phases, resulting in a phase diagram with 3 critical points and 4 amorphous phases. This multiplicity of amorphous phases is referred to as "polyamorphism",[29] in analogy to "polymorphism", the multiplicity of ordered crystal phases, such as occurs in many networked crystals like water and silica as well as in certain classes of ultrasoft materials like star polymers.[30]

Since the emergence of polyamorphism in the tetrahedrally functionalized NP is a consequence of the possibility to repeat interpenetrating tetrahedral structures, it is natural to ask whether such interpenetration can be effective when the network structure does not have a regular, repeating form. To probe this question, in this article we explore a model of NP functionalized with 3, 5, or 6 ssDNA with various directional arrangements. We find polyamorphous phase behavior for 5-armed NP with two different choices for the attachment orientation of the ssDNA, only one of which can form a geometrically regular space-filling network. For the 3-armed NP, we find only a single phase transition. For the 6-armed NP with octahedral symmetry, we find a hierarchy of at least six distinct crystal phases (polymorphism) and no stable amorphous phase transitions. This confirms that the cubic symmetry of the particle bonding sites imposes the same local bonding geometry on the crystal state, significantly lowering the nucleation rate.[31,32] Again, the possibility of nucleating a very open cubic crystal does not prevent the possibility of filling the remaining space with other interpenetrating ordered identical structures.

We demonstrate that the polyamorphism and polymorphism in all systems is the result of the interpenetration of multiple networks or lattices. Our findings are based on a series of Monte Carlo simulations of a generalization of the previously studied model for 4-armed NP complexes.[25,34] We describe the model and calculations in section 2. In section 3 we describe the results of the 3-, 4-, and 5-armed NP, which yield a phase diagram occupied by amorphous states, and in section 4 we examine the octahedral NP that exhibit hierarchies of cubic crystals. Our findings confirm that the extreme softness of these particles opens new possibilities for designing materials with interpenetrating networks in a very flexible structure.

2. Model and Simulation Methods

2.1. Model. To mimic nanosized particles grafted with a number of single strands of DNA studied experimentally,[23,24] ref 25 introduced a model of DNA dendrimer that has four single strands of DNA (ssDNA) tethered to a nanoparticle hub in a tetrahedral orientation. This model, which has also been adapted to describe complex DNA architectures like the Holliday junction,[33] captures the base-pair selectivity between two ssDNA and the bonding selectivity which ensures that each base can only bond to one other base. In this model, each DNA base, also described by a force site, is identified as either type A, T, C, or G, the standard abbreviation for the bases of DNA. Bases of type A can only bond with bases of type T; similarly, bases of type C can only bond with bases of type G. By choosing a palindromic base sequence, two ssDNA can bond in a head-to-tail order to form dsDNA. Strands are tethered to a nanoparticle hub that interacts via a short-ranged, purely repulsive potential to capture excluded volume effects. See ref 25 for a complete description.

This detailed model of base−base interaction is computationally costly for studying the bulk behavior due to the large number of force sites required. Therefore, an effective potential model was introduced through a coarse-graining study to simplify the original model.[34] This effective bonding potential between two ssDNA arms parametrizes the interactions of the original model using only the separation of the two nanoparticle cores and the relative angular orientation defined by the position of the DNA arms. With an additional lock-and-key condition imposed to mimic the bond selectivity that each arm combines with only one other ssDNA, this parametrized potential quantitatively reproduced the structure and phase behavior of the more complex model of NP functionalized with four ssDNA in a tetrahedral orientation.[27,34]

We use this effective nonadditive pair potential as a starting point and use the same form of the potential between DNA strands. To examine the effect of valency, we consider several choices for the number of ssDNA tethered to the nanoparticle cores, ranging from three to six, with distinct geometries. The DNA length is fixed to four bases. To reiterate, the model we use here is identical to that of ref 27, except for the number and direction of attached strands. Figure 1 summarizes the geometries of the macromolecular complexes we study: (a) the triangular planar (3-TP) are tethered with three ssDNA geometrically distributed on the same plane, 120° apart pairwise; (b) the tetrahedral geometry resembles the bond orientation of a carbon atom in a diamond lattice; (c) the square-based pyramid (5-SBP) structure has five ssDNA pointing to five vertexes of the square-based pyramid; (d) the triangle-based bipyramid (5-TBP) has the shape of sp^3d hybridized orbitals, equivalent to adding two additional ssDNA perpendicular to the previous 3-TP geometry; (e) the octahedral unit aligns six arms along orthogonal axis. The tetrahedral geometry has been discussed previously;[27] here we focus our attention on the other four geometries to investigate the valency dependence of phase behavior. The phase diagram corresponding to geometries (a)−(d) will be discussed in section 3, while the behavior of the octahedral units will be discussed in section 4. For reference, the total computational time for our study is estimated to amount to ≈15 months.

(25) Starr, F. W.; Sciortino, F. *J. Phys.: Condens. Matter* **2006**, *18*, L347–L353.
(26) Largo, J.; Starr, F. W.; Sciortino, F. *Langmuir* **2007**, *23*, 5896–5905.
(27) Hsu, C. W.; Largo, J.; Sciortino, F.; Starr, F. W. *Proc. Natl. Acad. Sci. U.S.A.* **2008**, *105*, 13711–13715.
(28) Bianchi, E.; Tartaglia, P.; Zaccarelli, E.; Sciortino, F. *J. Chem. Phys.* **2008**, *128*, 144504.
(29) Poole, P. H.; Grande, T.; Angell, C. A.; McMillan, P. F. *Science* **1997**, *17*, 322–323.
(30) Likos, C. N.; Löwen, H.; Watzlawek, M.; Abbas, B.; Jucknischke, O.; Allgaier, J.; Richter, D. *Phys. Rev. Lett.* **1998**, *80*, 4450–4453.
(31) Liu, H.; Kumar, S. K.; Douglas, J. F. *Phys. Rev. Lett.* **2009**, *103*, 018101.
(32) Noya, E. G.; Vega, C.; Doye, J. P. K.; Louis, A. A. *J. Chem. Phys.* **2007**, *127*, 054501.
(33) Ouldridge, T. E.; Johnston, L. G.; Louis, A. A.; Doye, J. P. K. *J. Chem. Phys.* **2009**, *130*, 065101.
(34) Largo, J.; Tartaglia, P.; Sciortino, F. *Phys. Rev. E* **2007**, *76*, 11402.

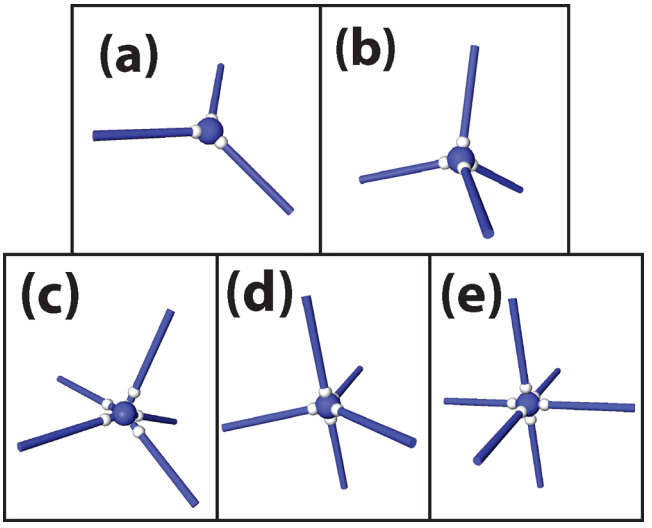

Figure 1. Cartoon of the geometries of the DNA-functionalized nanoparticles studied: (a) triangular planar (3-TP), (b) tetrahedral, (c) square-based pyramid (5-SBP), (d) triangle-based bipyramid (5-TBP), (e) octahedral. The central sphere indicates the NP, while the cylinder represents the sequence of DNA base pairs tethered to the central core at the small sphere locations.

2.2. Simulation Methods. For the amorphous systems, we first perform a series of Monte Carlo simulations in the grand canonical ensemble (fixed chemical potential μ, volume V, and temperature T) to coarsely map out the phase diagram from isotherms in the $\rho-\mu$ plane. Here we use reduced units defined by the effective potential.[35] Discontinuities of ρ indicate the approximate phase boundaries of a first-order phase transition. These results serve as a guide for more refined calculations, which we describe in the following.

To accurately locate the critical point, we select a state point that exhibits a bimodal density distribution $P(\rho)$, as $P(\rho)$ is known to be bimodal close to a second order critical point. Moreover, since the order parameter distribution $P(M)$ at the critical point for our system should follow the Ising universality class,[27] we apply a histogram reweighting scheme[36] to estimate the critical temperature T_c and critical chemical potential μ_c where $P(M)$ takes the expected form. Here $M = \rho - su$; u is the potential energy density and s is the field-mixing parameter. We carry out an additional simulation at the estimated T_c and μ_c and refine the estimate of T_c and μ_c again from histogram reweighting. We iterate this process until $P(M)$ converges to the form of the Ising class to within a very narrow tolerance.

Starting from the critical point and going down in T, we calculate $P(\rho)$ at phase coexistence using multicanonical sampling to *preweight* the sampling and artificially enhance the occurrence of switching between coexisting phases.[36] This requires that we first use histogram reweighting again to determine the appropriate μ for phase coexistence when we change T. The initial estimate for μ may require further refinement after performing an initial simulation. The densities of the coexisting phases can then be determined from the peaks of the $P(\rho)$ distribution at coexistence.

3. Amorphous Systems

3.1. Phase Behavior. We evaluate the phase behavior using the numerical procedure described in section 2 and locate the phase boundaries in the $T-\rho$ plane for the 3-TP, 5-TBP, and 5-SBP complexes (Figure 2) and include data for the tetrahedral dendrimer previously studied for comparison.[27] We find that 3-TP systems exhibit only one phase transition between unassociated molecules and a networked fluid state, analogous to a gas−liquid phase transition. We cannot formally rule out an additional phase transition at $T \leq 0.07$ (the lowest T investigated), but we do not expect any additional transition based on the relative transition temperatures for the 4- and 5-armed systems, which we now examine.

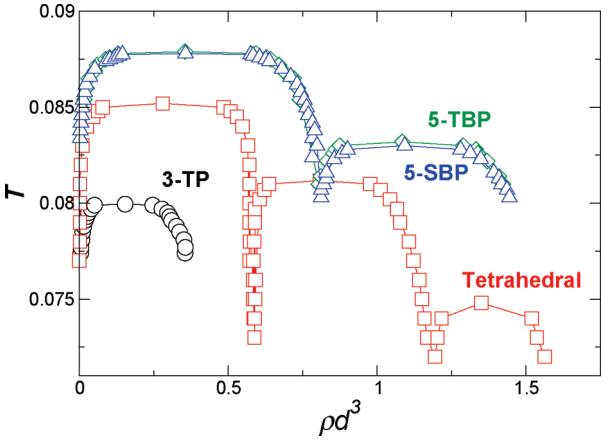

Figure 2. $T-\rho$ phase diagram of geometries 3-TP, tetrahedral, 5-TBP, and 5-SBP. The density is scaled by the cube of the bonding distance d^3 such that the density is comparable to the density of hard-sphere systems.

Both the 5-SBP and 5-TBP systems exhibit two critical points and three amorphous phases, as in the tetrahedral system, which has one more critical point and phase than the 5-armed systems. Simulations at larger ρ and low T for systems of both 5-armed nanoparticles show a rather sharp crossing between two states of different ρ, but we were unable to uncover unambiguous evidence that this crossover is discontinuous (i.e., not an additional first-order transition). In the previous study of the tetrahedral system, the occurrence of multiple critical points was explained by the formation of multiple interpenetrating networks. Our results indicate that multiple phase transitions can also occur for other geometries. But the question remains: do the multiple transitions occur in the 5-armed systems by constructing interpenetrating networks or by some other means. We will address this question in the next section examining the structure.

The locations of the critical points of both the gas−liquid and liquid−liquid phase transitions decrease in both ρ and T as the valency decreases, and coexistence regions become smaller. These findings are in agreement with previous findings for the liquid−gas transition of systems with limited valency γ.[28,37] To our knowledge, this is the first time the effect of valency on the liquid−liquid transitions has been examined. The decrease of T_c with decreasing γ can be understood from the fact that, with fewer bonding arms, the total binding energy of a networked state is smaller. Accordingly, less thermal energy is required to break up the network into a gaslike phase. The decrease of ρ_c with decreasing γ can be understood from the fact that, with fewer bonding arms, fully bonded structures require lower densities. The decrease of density for low valency particles was suggested to provide an equilibrium route, as opposed to phase separation,[38]

(35) The reduced units are defined in terms of the detailed model in ref 25, where length is in units of an effective base diameter, energy is in units of base-pair attraction ε, and T is in units of ε/k_B.
(36) Wilding, N. B. *Am. J. Phys.* **2001**, *69*, 1147–1155.
(37) Sastry, S.; La Nave, E.; Sciortino, F. *J. Stat. Mech.* **2006**, 12010.
(38) Lu, P. J.; Zaccarelli, E.; Ciulla, F.; Schofield, A. B.; Sciortino, F.; Weitz, D. A. *Nature* **2008**, *453*, 499–503.

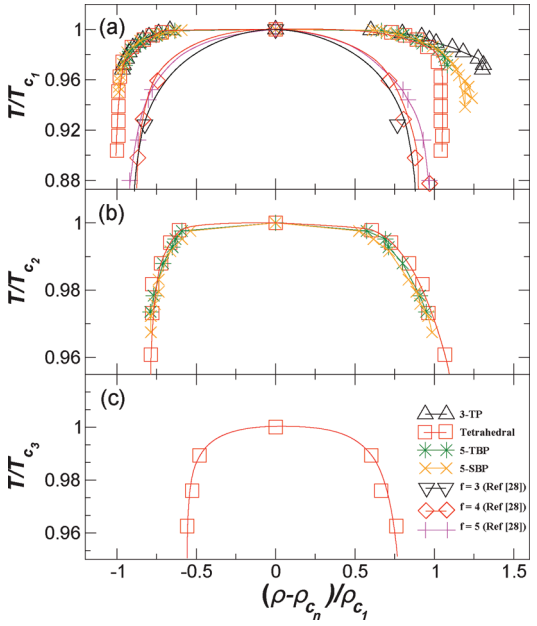

Figure 3. $T-\rho$ phase diagram with density shifted by respective critical densities and scaled by first critical density; the temperature is scaled by the respective T_c. The solid lines are guides to the eye. (a) The first phase transition, analogous to a gas−liquid transition, for geometries 3-TP, tetrahedral, 5-TBP, and 5-SBP. In addition, we show results from patchy colloids from reference with either 3, 4, or 5 patches.[28] (b) The second phase transition, a liquid−liquid phase transition, for geometries 5-TBP, 5-SBP, and tetrahedral. (c) The third phase transition for tetrahedral geometry.

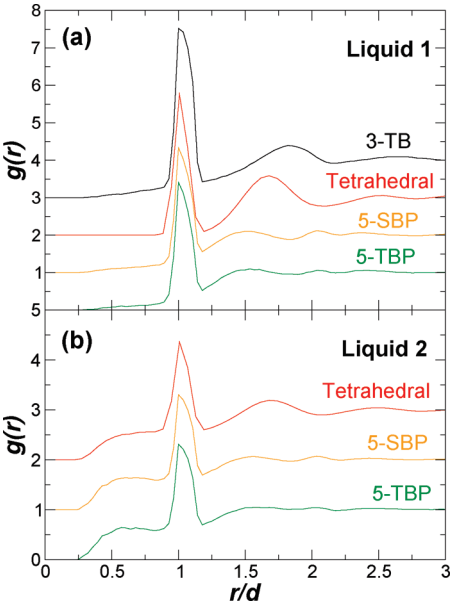

Figure 4. Radial distribution function $g(r)$ as a function of scaled distance r/d, where d is the typical bonding distance. For visual clarity, $g(r)$ for 5-SBP, tetrahedral, and 3-TB are shifted vertically by 1, 2, and 3, respectively. (a) $g(r)$ of the first liquid, including geometries 3-TB ($T=0.08$, $\rho d^3=0.28$), tetrahedral ($T=0.073$, $\rho d^3=0.64$), 5-SBP ($T=0.0826$, $\rho d^3=0.86$), and 5-TBP ($T=0.0825$, $\rho d^3=0.82$). (b) $g(r)$ of the second liquid, including tetrahedral ($T=0.073$, $\rho d^3=1.29$), 5-SBP ($T=0.0826$, $\rho d^3=1.43$), and 5-TBP ($T=0.082\,50$, $\rho d^3=1.44$).

to gel formation in the context of short-range particle interactions.[39,40] This work demonstrates that a strong thermodynamic driving force for phase separation—competing with the formation of equilibrium gels—may be present even for densities larger than the gas−liquid typical densities when the softness of the potential allows for formation of interpenetrating fully bonded networks via the onset of additional phase separations. Moreover, our results suggest that this unexpected phenomenon does not require a specific valence or a specific orientation and can be exhibited by nanoparticles with more complex interactions.

The two geometries with $\gamma=5$ exhibit phase boundaries that are nearly quantitatively identical, indicating that the phase behavior is not sensitive to geometric differences of the molecular units we have studied. This result agrees with previous study of systems of hard-sphere patchy particles with either fixed or random location of the patches.[28] However, in the patchy hard sphere system—where nearest-neighbor distances are controlled by the hard-core diameter and not by the bonding—only one phase transition is observed. If binding can occur in any direction, it will be possible to form all bonds at nearly any liquidlike ρ. With specific orientation of the arms, not all bonds may be possible in some density ranges, potentially creating a thermodynamic drive to separate into coexisting phases which are each fully bonded. In other words, the specificity in distances and orientations required for bonding introduces a strong coupling between the energy of the system and its density, thus establishing optimal density values where fully bonded states can be achieved.[41]

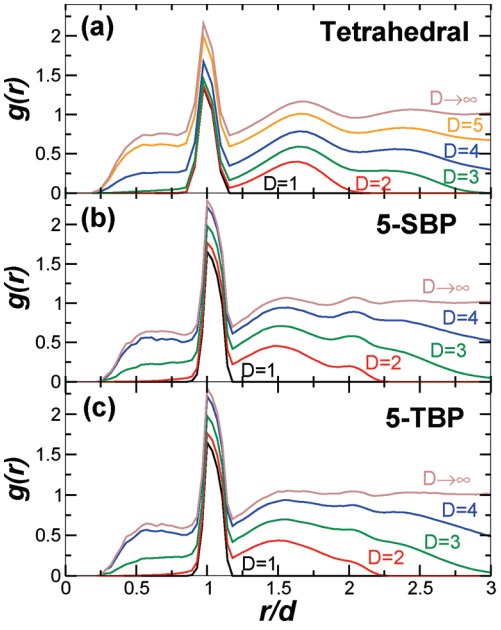

Figure 5. $g(r)$ restricted to bonded neighbors up to a specific chemical distance D for the second liquid of (a) tetrahedral geometry ($T=0.073$, $\rho d^3=1.29$), (b) 5-SBP ($T=0.0826$, $\rho d^3=1.43$), and (c) 5-TBP ($T=0.0825$, $\rho d^3=1.44$).

To assess how the shape of the coexistence curves depends on valency, we examine a scaled version of the phase diagram in Figure 3. Specifically, we first scale T by the respective critical temperature of each transition. We then shift ρ by ρ_c for each transition separately; we then scale by critical density of the first phase transition so that the widths of the coexistence regions are comparable. Results from ref 28 are also added to Figure 3a to

(39) Zaccarelli, E.; Buldyrev, S. V.; La Nave, E.; Moreno, A. J.; Saika-Voivod, I.; Sciortino, F.; Tartaglia, P. *Phys. Rev. Lett.* **2005**, *94*, 218301.
(40) Bianchi, E.; Largo, J.; Tartaglia, P.; Zaccarelli, E.; Sciortino, F. *Phys. Rev. Lett.* **2006**, *97*, 168301.
(41) De Michele, C.; Gabrielli, S.; Tartaglia, P.; Sciortino, F. *J. Phys. Chem. B* **2006**, *110*, 8064.

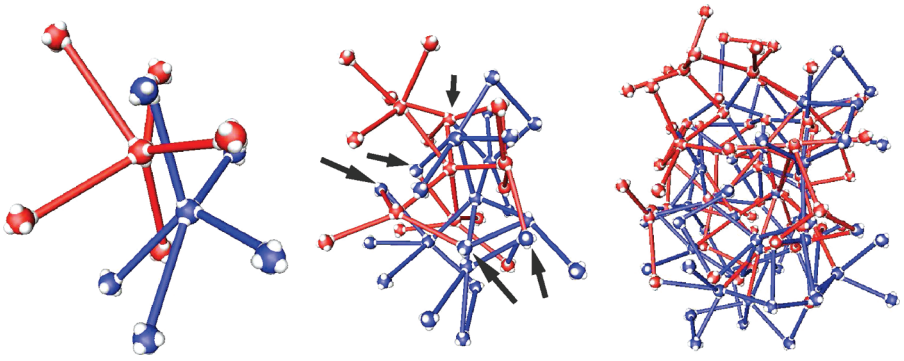

Figure 6. Visualization of the two interpenetrating networks up to chemical distance $D = 1$, $D = 2$, and $D = 3$ for 5-SBP at $T = 0.0826$, $\rho d^3 = 1.44$. We assign two different colors to illustrate the two distinct interpenetrating networks. The arrows indicate locations where the two networks intersect each other as a result of distortion.

facilitate the comparison of the phase boundary of the ssDNA-armed nanoparticles with that of the colloids functionalized with 3, 4, or 5 geometrically distributed "sticky patches" that serve as bonding sites.[28]

For the DNA system, the shape of the liquid−gas phase boundary near T_c is largely insensitive to the number of arms. Further from the critical point, the 3-armed system appears widest, consistent with the patchy colloid system (although the difference in width for the patchy colloidal system occurs further from the critical point, outside our plot range). The phase boundary for the second transition (in the 5-TBP, 5-SBP, and tetrahedral systems) appears largely insensitive to the number or orientation of the arms. However, we should be careful to point out that the data only cover a small range near the critical point; further from T_c, the phase boundaries may differ. For reference, we also show the third transition for the tetrahedral system.

We note that there is a clear difference in phase boundaries of the DNA and patchy colloid systems, which can be explained by the nature of DNA bonding. In our model, the DNA arm bonding process requires simultaneous bonding of a sequence of four DNA bases. This high degree of cooperativity in bonding yields a much larger enthalpy and entropy change on bonding than for the patchy colloids. Accordingly, the phase separation occurs over a very narrow window, flattening the phase boundary near the critical point.

3.2. Structure. We now examine the fluid structure to determine whether the second phase transition in the 5-SBP and 5-TBP systems arise through network interpenetration, as previously shown for the tetrahedral system.[27] As a first step in this direction, we calculate the radial distribution $g(r)$, where r is the separation between the centers of particles. We show $g(r)$ for the first networked liquid (i.e., for the phase coexisting with the gas) for all geometries in Figure 4a; we show $g(r)$ for the second network liquid for the tetrahedral, 5-SBP, and 5-TBP systems in Figure 4b. The separation r is scaled by d, the typical bonding distance, so that the first peak (the separation of the first bonded neighbor) is at $r/d = 1$. For the tetrahedral system, the second-neighbor peak occurs at $4/\sqrt{6} \approx 1.63$ times the position of the first-neighbor peak, typical for an ideal tetrahedral coordination. In contrast, $g(r)$ for the single network formed by 3-TP has a broader second peak at $r/d \approx \sqrt{3} \approx 1.8$, consistent with the 120° angle between two arms. For the 5-SBP and 5-TBP systems there is a very weak and broad second peak at $r/d \approx 1.5$. This clarifies that the 3- and 5-armed systems do *not* form networks with a locally tetrahedral order.

The structural difference between single networks of tetrahedral and the other geometries can also be observed in the region $r/d < 1$. Specifically, for the tetrahedral structure, $g(r)$ is identically zero for $r/d \lesssim 0.8$, while 3-TP, 5-SBP, and 5-TBP have a small amplitude for $0.25 \lesssim r/d \lesssim 0.8$, signifying the presence of molecules at distance closer than first-bonding neighbors. Accordingly, the structures of these networks are far less regular than the tetrahedral system.

For the second liquid of the polyamorphous systems (Figure 4b), we observe a significant increase in $g(r)$ for the region $r/d < 1$. The large increase of particles at distances less than the first-neighbor binding distance is consistent with the presence of a complementary network that interpenetrates the first one. Such interpenetration is possible due to the short-range of core repulsion compared to the bonding distance. Structural features similar to those of the first liquid can be observed in the second liquid: the second peaks of tetrahedral geometries, 5-SBP, and 5-TBP occur roughly at the same positions as the first liquids of each geometry but become slightly broader. The preservation of signatures of $g(r)$ suggests a similar structure of each of the interpenetrating networks.

To demonstrate that interpenetrating networks preserve their structure locally, we examine the $g(r)$ restricted to nanoparticles that are separated by a specific number of bonds, referred as chemical distance D (Figure 5). More specifically, $g(r)$ for $D = 1$ only shows the correlations with the nearest bonded neighbors, while $D = 2$ includes both the first and second bonded neighbors, etc. In this way, we can calculate the correlation only among the bonded neighboring particles that are separated by no more than D bonds. The ordinary $g(r)$ is recovered in the limit $D \to \infty$.

The difference between the networks formed by the tetrahedral system and the two 5-armed systems is best demonstrated by examining $g(r)$ for $D = 2$. For the tetrahedral system, the second bonded neighbor has a well-defined peak position, determined by the tetrahedral network. For the 5-SBP and 5-TBP systems, $g(r)$ at $D = 2$ shows *two* distinct peaks for the possible location of the second bonded neighbor. This further demonstrates that these systems form a less sharply defined network than the tetrahedral system. Differences in the network geometries can also be observed in $g(r)$ for region $r/d < 1$. Since the restricted $g(r)$ only considers bonded neighbors, the increase at region $r/d < 1$ is a contribution from particles of the same network that loop back to very small physical distance r. For tetrahedral networks, a significant increase of $g(r)$ at region $r/d < 1$ only occurs at $D \geq 4$, whereas for 5-SBP and 5-TBP systems, the increase takes place at $D \geq 3$. This shows that the 5-armed particles loop back more easily than the tetrahedral geometry, consistent with a more distorted network.

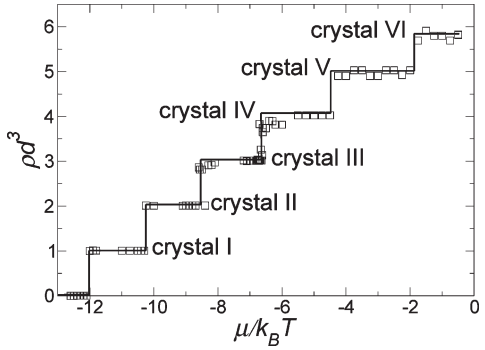

Figure 7. $\rho-\mu$ diagram of six crystals at $T = 0.083\,11$. The density is scaled by d^3, where d is the typical bonding distance. The line is a guide to the eye.

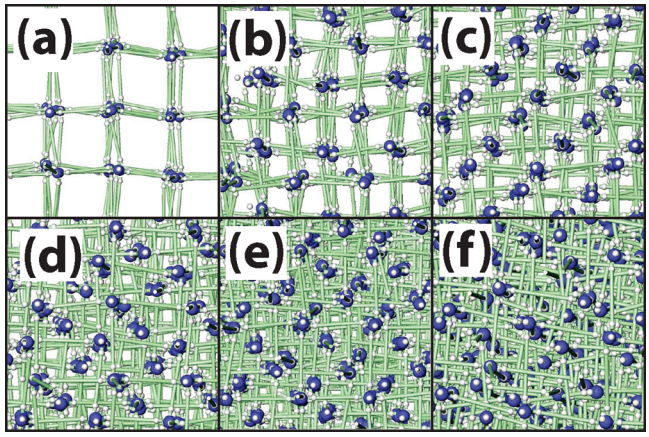

Figure 8. Visualization of the interpenetrating lattices of (a) crystal I ($T = 0.083\,11$, $\rho d^3 = 1.0$), (b) crystal II ($T = 0.083\,11$, $\rho d^3 = 2.0$), (c) crystal III ($T = 0.083\,11$, $\rho d^3 = 3.0$), (d) crystal IV ($T = 0.083\,11$, $\rho d^3 = 4.0$), (e) crystal V ($T = 0.083\,11$, $\rho d^3 = 5.0$), and (f) crystal VI ($T = 0.083\,10$, $\rho d^3 = 6.03$). Specifically, in (b), the core of a DNA complex locates roughly in the center of the other lattice unit cell, a result of two interpenetrating lattices. Because of the large amount of empty space, this motif can be repeated.

Finally, we can explicitly show the interpenetration by drawing two neighboring but disconnected DNA complex cores with the associated networks up to $D = 1$, $D = 2$, and $D = 3$ for a system of 5-functionalized NP at the region of high ρ and low T (Figure 6). The two different colors indicate two interpenetrating networks. For $D = 1$, the two interpenetrating networks separate cleanly (Figure 6a). However, when $D = 2$, two networks are connected at five points. We can also observe a closed loop in the blue network on the top right in Figure 6b. The two networks are further distorted at $D = 3$. Some red NP are connected to multiple blue bonds, and vice versa, suggesting the interconnectedness of the two networks. Nonetheless, a large portion of the two networks are distinct and can be easily identified. From the rapid growth of the entanglement, it is clear that the interpenetration of two networks is a local trait which looses sharpness at long range.

4. Crystal System

Unlike the other geometries which make disordered networked states, the system of DNA complexes with octahedral geometry (Figure 1e) readily forms an ordered crystal lattice. The octahedral geometry naturally lends itself to the formation of networks with cubic symmetry, as noted previously in studies of patchy colloids with six interacting sites.[32,31] Simulations indicate a transient amorphous phase is possible, but it rapidly crystallizes.

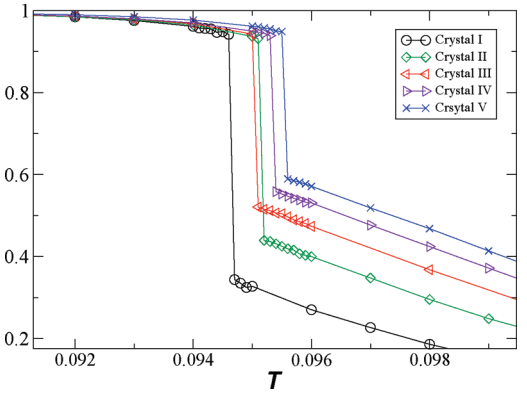

Figure 9. Percentage of intact bonds as a function of T on heating for crystals I−V. The discontinuity provides an upper limit on the melting temperature.

The lowest density crystal phase, which we call crystal I, has $\rho d^3 = 1$. This cubic geometry has a complementary lattice of holes that is also cubic, which should allow for the possibility of interpenetrating crystal networks. Indeed, Figure 7 shows that, by increasing μ at fixed T, we can observe a series of up to six thermodynamically distinct polymorphous phases. Each subsequent crystal has density equal to integer multiples of the density of crystal I, suggesting repetitions of the crystal I lattice. The visualization of each crystal shows that the system is indeed forming hierarchies of interpenetrating simple cubic lattices (Figure 8). The density of each crystal state stays nearly constant throughout a range of μ, followed by a sudden jump at a threshold μ, making a higher density crystal. This suggests only a very narrow range of stable densities for each crystal. Crystal VI is the highest density crystal we obtained. High-density crystals beyond crystal VI might exist, but as more cores of the particle reside in a lattice unit cell, the core−core interactions may frustrate the formation of higher density crystals.

To map out the phase behavior of these crystals, we estimate an upper bound for the melting temperatures of each crystal. We anneal the crystal at a series of increasing T at fixed density until there is a discontinuous melting (Figure 9). This likely overestimates the thermodynamic melting temperature. Using the estimated melting temperatures, we plot the phase diagram in Figure 10. The shaded areas between the narrow stable regions are phase coexistence regions. The phase boundaries of other geometries are partially drawn in scale on the bottom left corner in the graph for comparison.

The melting temperatures increase as the system reaches higher density with more interpenetrating lattices, contrary to other polyamorphous geometries which have lower T_c for transitions between phases with more interpenetrating networks. This would be expected if the higher density crystals were able to form with fewer defects and hence a *lower* energy per site. However, our numerical data show that the energy per site for the higher density crystals is progressively *higher* and hence less energetically stable. Instead, we can understand the density dependence from the perspective of the Lindemann criterion,[42] i.e., that a crystal typically melts when its vibrational amplitude reaches a critical fraction of the bond length. The repeated interpenetration of disconnected networks reduces the available space and correspondingly decreases the vibrational amplitude, while the bond length remains unchanged. As a result, the higher density crystal will only melt at higher T. In contrast, for other polyamorphous

(42) Lindemann, F. A. *Z. Phys.* **1910**, *11*, 609.

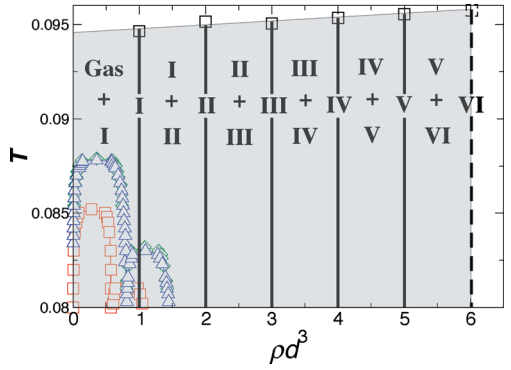

Figure 10. $T-\rho$ phase diagram of multiple crystals formed by octahedral nanoparticles. The density is scaled by d^3. The gray regions indicate phase coexistence between crystals, except for the smallest density, where crystal I coexists with the gas phase. Crystal VI is observed, but we are not able to obtain a reliable melting temperature, and therefore represented by the dashed lines. For comparison, we also show phase boundaries of the amorphous systems obtained in Figure 2: red squares are for the tetrahedral orientation; blue triangles are for the 5-SBP; green diamonds are for the 5-TBP.

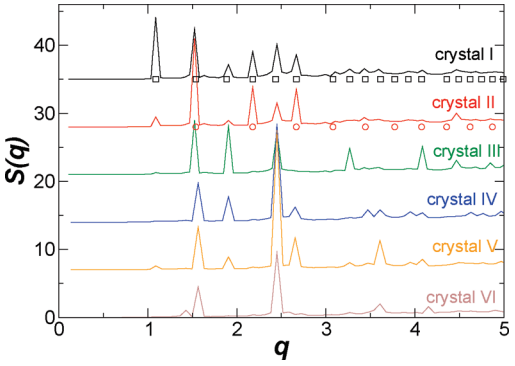

Figure 11. $S(q)$ for octahedral geometry. For clarity, lines are shifted vertically so that each crystal is 7 units apart. The black squares below crystal I are the theoretically expected locations for the peaks of a perfect simple cubic lattice; similarly, the red circles below crystal II are the expected locations for the peaks of a perfect BCC lattice.

geometries, the formation of the second interpenetrating network unavoidably distorts and destabilizes the first network, making both networks more susceptible to high temperature, thereby depressing T_c.

To quantify the crystal structure, we calculate the structure factor $S(q)$ (Figure 11). The sharp peaks exhibited by all densities of crystals are indicators of ordered crystals, consistent with the interpenetration of well-defined crystal I in higher density crystals. Specifically, based on the visualization snapshots (Figure 8) and the fact that octahedral geometry tends to construct simple cubic lattice, we expect crystal I to be simple cubic lattice and crystal II to have DNA complex cores located at BCC lattice sites. This is confirmed by including the theoretical values for the peak positions for a simple cubic lattice for crystal I and the theoretical values for peak positions of a BCC lattice for crystal II.[43] In the region $q \lesssim 2.8$, the peak locations of both crystal I and II match the predicted q values for SC and BCC lattice. Furthermore, the amplitude of $S(q)$ for crystal II is around twice that of crystal I at corresponding q values, in agreement with the theoretical prediction. There are peaks in $S(q)$ of crystal II at region $q \lesssim 2.8$ which are not predicted by the theoretical calculation. They occur at q values predicted for crystal I but have much smaller amplitude, suggesting that they are residual traits of crystal I, which did not die out completely due to the imperfections of crystal II.

5. Discussion and Conclusions

We have demonstrated that DNA-functionalized nanoparticles with several different numbers of DNA-arms and different directionalities exhibit a rich phase behavior: the tetrahedral geometry forms four amorphous phases accompanied by three first-order critical points; the 5-SBP and 5-TBP have three amorphous phases accompanied by two critical points; the octahedral geometry makes at least six polymorphous crystals. The common motif for all geometries is the repetition of networks that utilize the empty spaces in other networks and therefore interpenetrate each other. Indeed, such interpenetrating lattices occur in nature in crystal forms, such as in ice VI, VII, and VIII.[44] This interpenetration likely also plays a secondary role in the hypothesized liquid−liquid transition of water.[45,46] We expect the interpenetration of networks is more limited in traditional molecular systems than in our DNA-functionalized nanoparticles, since, unlike the DNA system, the range of attraction between molecules is only slightly larger than the core repulsion size. Such short bond distances (as compared to the repulsive core size) provides limited empty space, and significant hard-core interactions frustrate the formation of additional interpenetrating networks. Conversely, for longer ssDNA (provided the length is shorter than the persistence length), even further repetition of the interpenetration process may be possible.

In our system we find the phase coexistence region shrinks as the valency γ decreases, in agreement with previous studies.[28,37] As a result, the limited valency opens a large region of densities that can be occupied by the complementary networks. The emergence of thermodynamically distinct phases at higher density appears to rely on the specific directionality of bonding interactions. Indeed, systems with only limited valency do not show additional phase transitions. The directionality is further enhanced by the lock-and-key mechanism of DNA that ensures one bond per bonding site, as opposed to systems where multiple bonding sites may form simultaneous pairs of bonds. Such multiple bonding would lead (i) to a more crowded local environment with associated distortion of the network and absence of the empty space and (ii) to the possibility of additional interactions between distinct networks. Indeed, the lock-and-key interaction is a fundamental ingredient since it is responsible of the inertness of the network which condenses from the phase separation process. Experimentally, DNA strands have a weak electrostatic repulsion. It has been argued[47] that weak repulsion between bonding strands would favor more ordered structures and reduce the probability of self-assembling into an undesirable structures. This should reduce distortions of the network, thereby facilitating the interpenetration process. Additionally, due to the helical pitch of ≈10 base pairs of DNA, it may be experimentally important to consider multiples of 10 bases to avoid stress that might distort the regularity of the structure.

(43) Kittel, C. *Introduction to Solid State Physics*; Wiley Publishers: Hoboken, 2005.
(44) Fletcher, N. H. *The Chemical Physics of Ice*; Cambridge University Press: Cambridge, 1970.
(45) Poole, P. H.; Sciortino, F.; Essmann, U.; Stanley, H. E. *Nature* **1992**, *360*, 324–328.
(46) Mishima, O.; Stanley, H. E. *Nature* **1998**, *392*, 164–168.
(47) Licata, N. A.; Tkachenko, A. V. *Phys. Rev. E* **2006**, 74.

The regularity of the tetrahedral and octahedral systems facilitates interpenetration. For the 5-SBP system, there is no regular space-filling network possible, and thus the distortion obstructs the formation of other complementary networks. Nonetheless, the system can still undergo two amorphous phase transitions and construct two interpenetrating networks due to the ample empty space. The system can potentially form a third network, but unlike the tetrahedral system, we did not observe a clear phase separation in the corresponding high-density region. In principle, the 5-TBP system could form connected hexagonal sheets, although we never observed such an ordered state. While this structure could tile space, it does not promote interpenetration, since the voids of such a network are dissimilar from the original network. As a result, we observe behavior nearly identical to that of the 5-SBP system. For the octahedral system, a well-defined ordered lattice allows the interpenetration of networks to occur more easily. We observed 6 interpenetrating simple cubic lattices, compared with only 3 and 2 networks found in the amorphous 4-armed and 5-armed systems, respectively.

The formation of low-density NP assemblies with crystalline order is expected to be an important step toward the development of new materials with unusual optical or electronic properties.[48,49] Moreover, the possibility of multiple distinct networks should expand the potential applications. For example, increasing the number of interpenetrating networks changes the lattice spacing and thus the scattering properties. Alternatively, distinct networks might serve as separate, but interwoven, change transfer conduits for electronic materials.

Acknowledgment. We thank J. Douglas and J. Largo for helpful discussions and thank Wesleyan University for computer time, which was supported by National Science Foundation Grant CNS-0619508. This work was supported by National Science Foundation Grant DMR-0427239. F. Sciortino acknowledges support from ERC-226207-PATCHYCOLLOIDS.

(48) Crocker, J. C. *Nature* **2008**, *451*, 528–529.
(49) Osakada, Y.; Kawai, K.; Fujitsuka, M.; Majima, T. *Proc. Natl. Acad. Sci. U.S.A.* **2006**, *103*, 18072–18076.